

# Dissipation Potentials for Yarn-Level Cloth

Rosa M. Sánchez-Banderas Miguel A. Otaduy

Universidad Rey Juan Carlos, Madrid



Figure 1: A mannequin wearing a tank top. Thanks to our proposed damping model, the motion of the garment remains nicely damped even under fast motion of the mannequin, yet the fabric retains rich folds and wrinkles.

## Abstract

*Damping is a critical phenomenon in determining the dynamic behavior of animated objects. For yarn-level cloth models, setting the correct damping behavior is particularly complicated, because common damping models in computer graphics do not account for the mixed Eulerian-Lagrangian discretization of efficient yarn-level models. In this paper, we show how to derive a damping model for yarn-level cloth from dissipation potentials. We develop specific formulations for the deformation modes present in yarn-level cloth, circumventing various numerical difficulties. We show that the proposed model enables independent control of the damping behavior of each deformation mode, unlike other previous models.*

## CCS Concepts

•*Computing methodologies → Physical simulation;*

## 1. Introduction

In mechanics, damping is the dissipation of energy stored in oscillating systems. This dissipation is produced by complex interactions, such as friction, and ultimately the resistance of matter to change its current shape or structure. Popular materials in computer graphics exhibit highly varying damping behaviors, from the inviscid behavior of water to the highly damped behavior of flesh. Accurate modeling of dissipative properties is key for achieving realistic dynamic simulation of real-world phenomena.

In computer graphics, the simulation of viscoelastic fluids has received ample attention [GBO04, PICT15]. For solids, on the other hand, damping has often been overlooked in contrast to elasticity. Many solid simulation works simply rely on the numerical damping produced by implicit integrators, or they implement linear damping models [OSG02, BJ05, CLMMO14, GSS\*15]. However, some authors have paid attention to the design of good dissipation models for solids. Baraff and Witkin [BW98] defined damping forces

aligned with elastic forces, but proportional to time-derivatives of position constraints. Their proposed model bears a strong connection to dissipation potentials in classical mechanics [GPS14], even though this connection went unnoticed to them. The design of damping forces has also received attention under research on variational integrators [KYT\*06, GSS\*15], or for simple control of dissipation properties in animation [SSF13].

In this paper, we focus on the dissipative behavior of yarn-level cloth models [KJM08, KJM10]. In particular, the efficient yarn-level model by Cirio et al. [CLMMO14, CLMO15, CLMO17], which represents cloth as a structure of flexible rods with sliding persistent contacts. Yarn-level cloth models enable the simulation of realistic small-scale fabric effects, such as snags, loose yarn ends, or detailed fracture, and they also reproduce the macroscopic nonlinear mechanics of garments simply by aggregating yarn-level structural effects. However, the model of Cirio et al. achieves high efficiency through a mixed Eulerian-Lagrangian dis-

cretization, which complicates the application of common dissipation models in computer graphics.

The contributions of our work are:

- Application of dissipation potentials to yarn-level cloth, including the design of specific dissipation potentials to damp the energy stored on the various conservative potentials of yarn-level cloth mechanics.
- Derivation of dissipative forces and their Jacobians for mixed Eulerian-Lagrangian discretizations. A key aspect is the formulation of dissipation potentials as quantities integrated along yarns, which unveils the structure of Eulerian dissipative forces and their Jacobians.
- Robust formulation of dissipative forces for angular potentials. We have recognized that naïve bending and shear dissipative forces suffer from indeterminacy at small angles. As a solution, we propose a vector form of bending and shear strain for small angles, which is free of indeterminacy, and whose dissipation potential smoothly blends into the regular dissipation potential based on scalar forms of strain.
- Discussion of the differences w.r.t. other damping models. We analyze the application of full linear Rayleigh damping and the damping approach of Baraff and Witkin [BW98] to mixed Eulerian-Lagrangian discretizations, and we conclude that they produce undesirable forces which do not correctly model dissipation.
- Experimental analysis of practical damping properties. With our formulation based on dissipation potentials it is possible to control independently the damping behavior of different deformation modes. We have validated this fact by analyzing the correlation of the damping ratio for different deformation modes.

We continue the paper with a discussion of related work, followed by a review of the derivation of the equations of motion for yarn-level cloth mechanics. Then, we introduce a generic formulation of dissipation potentials as integrated quantities, and we derive the corresponding forces and Jacobians for mixed Eulerian-Lagrangian discretizations. Next, we formulate specific dissipation potentials for yarn-level cloth, and we describe our theoretical and experimental analysis.

## 2. Related Work

Characterization of damping mechanisms in dynamics simulation is an active area of research. It is fundamental for achieving realistic behavior of real-world materials and to improve the stability of the simulated systems. However, despite the large amount of research, understanding of damping mechanisms remains primitive.

A major reason for this is that, in contrast with inertia and stiffness forces, it is not clear which state variables are relevant to determine the damping forces. By far the most common approach is to assume so-called ‘viscous damping’, where only the instantaneous velocities are the relevant state variables that determine damping.

This idealization is widely discussed in the literature of Lagrangian mechanics [GPS14], where the appearance of such forces is formalized through the so-called dissipative potentials or velocity-dependent potentials, as well as Rayleigh’s dissipation function.

Physical models usually distinguish three distinct types of damping, depending on their nature and purpose. (i) Damping that is deliberately formulated in order to simulate the nature of the given material is often referred to as *material-intrinsic damping* [CK05]. (ii) Damping produced by implicit formulations of the system dynamics is referred to as *artificial* or *numerical damping*. (iii) Damping added to enhance stability is usually referred to as *fictitious damping* [YKC00].

One of the first works that recognized the need of damping forces in cloth simulation was developed by Terzopoulos et al. [TPBF87], where the cloth was discretized as a rectangular mesh and energy functions were derived using a continuum formulation. However, they only implemented a simple viscous drag force, hence their damping function dissipated all kinetic energy, regardless the type of motion.

Following the treatment of deformable surfaces by Terzopoulos et al., Carignan et al. [CYTT92] described a cloth simulation system using a rectangular discretization. They recognized the need for damping functions which do not penalize rigid-body motions of the cloth (unlike simple viscous damping), hence they added a force which damps cloth stretch and shear (but not bending). Nevertheless, their damping function—a linear function of velocity—does not match the quartic energy functions of their continuum formulation.

Baraff and Witkin [BW98] described a general treatment for damping that was independent of the specific energy function being damped. They defined elastic potentials based on soft constraints, and then they modeled dissipative forces simply by replacing the constraint values of elastic forces with constraint derivatives. Their method avoids unnecessary dissipation of the system’s total kinetic energy. Bender and Deu [BD13] also used this type of damping for adaptive cloth simulation with corotational finite elements. Following up the work of Baraff and Witkin, Oh et al. [OAW06] proposed an implicit integration technique that is able to reproduce stable cloth without introducing excessive damping forces. Artificial internal damping forces are generated during the linearization process of their semi-implicit integrator. Despite its generality, the method of Baraff and Witkin is not directly applicable to the yarn-level cloth model of Cirio et al. [CLMM014, CLMO15, CLMO17], due to the mixed Eulerian-Lagrangian discretization, which introduces additional terms in elastic forces.

Volino and Magnenat-Thalmann [VMT00, VMT01] found that damping forces can lead to systems in which wrinkles do not form on the surface of the cloth, wrinkles resist disappearing, or the fabrics even resist falling under their own weight. Choi and Ko [CK05] proposed a method that includes artificial damping and material intrinsic damping, but does not include fictitious damping. They avoid the need for fictitious damping through the use of a predicted static post-buckling response as an effective way of handling the instabilities associated with post-buckling situations.

Other cloth simulation works opted for the use of Rayleigh damping [Ray96], which is a commonly used approach to model dissipative forces in complex engineering. In essence, it is a viscous damping force proportional to a linear combination of the mass and stiffness matrices. This model was used by Grispu et al. [GHDS03] with a Newmark ODE integration scheme, and by

Cirio et al. [CLMMO14] with backward Euler implicit integration. However, stiffness-proportional damping includes undesirable terms that lead to an underwhelming loss of kinetic energy.

### 3. Equations of Motion of Yarn-Level Cloth

As mentioned in the introduction, the yarn-level cloth model of Cirio et al. [CLMMO14, CLMO17] uses a generalized-coordinate representation that combines both Eulerian and Lagrangian coordinates. The yarns are sampled at their permanent contacts, and each contact is described by its 3D position  $\mathbf{x}$  and the arc-length positions  $(u, v)$  within the two yarns in contact. The 3D position of the contact can be regarded as the Lagrangian part of the discretization, and the arc-length positions can be regarded as the Eulerian part. In practice, the addition of arc-length coordinates as degrees of freedom enables the simulation of persistent contacts with sliding. Inter-yarn contact is handled implicitly, avoiding altogether the computation of collision detection and collision response between yarns that are permanently in contact.

The combined Lagrangian and Eulerian generalized coordinates form a set of *reduced* coordinates  $\mathbf{q}$ . The 6D configuration space of two points in contact is constrained to 5D by removing the degree of freedom normal to the two yarns. In this reduced-coordinate setting, the equations of motion that describe the dynamic evolution of a garment are derived from the Lagrangian, as Euler-Lagrange equations [GPS14].

With a conservative potential  $V$  and kinetic energy  $T = \frac{1}{2} \dot{\mathbf{q}}^T \mathbf{M} \dot{\mathbf{q}}$ , the Euler-Lagrange equations are:

$$\mathbf{M} \ddot{\mathbf{q}} = \nabla T - \nabla V - \dot{\mathbf{M}} \dot{\mathbf{q}}. \quad (1)$$

The definition of the mass matrix  $\mathbf{M}$  for yarn-level cloth is given in [CLMMO14].

For a discrete element with strain  $\epsilon$  and size  $\Omega$ , a generic quadratic elastic potential with stiffness  $k_e$  can be expressed as

$$V = \frac{1}{2} \Omega k_e \epsilon^2. \quad (2)$$

The specific conservative potentials for woven and knitted cloth are defined, respectively, in [CLMMO14] and [CLMO17], but later in Section 5 we review some of them for the definition of dissipation potentials.

From (2), the conservative (elastic) force on the generalized coordinates can be written as:

$$\mathbf{f}_e = -\nabla V = -\Omega k_e \epsilon \nabla \epsilon - \frac{1}{2} k_e \epsilon^2 \nabla \Omega. \quad (3)$$

The force proportional to  $\nabla \Omega$  is due to the presence of Eulerian coordinates, and is not present under purely Lagrangian discretizations.

Baraff and Witkin [BW98] designed dissipative forces by preserving the direction of elastic forces and substituting their magnitude with a term dependent on the strain rate  $\dot{\epsilon}$ . Under the mixed Eulerian-Lagrangian discretization, the elastic force exhibits two terms, as shown above. As it will become evident in Section 4.2, only the term proportional to  $\nabla \epsilon$  should contribute to dissipation. Moreover, Baraff and Witkin did not pay attention to the definition

of dimension-less strains. They built the element size  $\Omega$  partly in the stiffness constant and partly in the strain metric. With Eulerian coordinates, where the sizes of elements change during the simulation, this would lead to important errors.

Cirio et al. [CLMMO14] added damping to yarn-level cloth using the Rayleigh model. Specifically, they modeled a damping force

$$\mathbf{f}_d = - \left( \alpha \mathbf{M} - \beta \frac{\partial \mathbf{f}_e}{\partial \mathbf{q}} \right) \dot{\mathbf{q}}, \quad (4)$$

with parameters  $\alpha$  and  $\beta$  controlling, respectively, the dissipation of absolute and relative velocities. When applied to a mixed Eulerian-Lagrangian discretization, the Rayleigh damping force contributes a term dependent on  $\nabla \Omega$  from (3). Again, as it will become evident in Section 4.2, only the term proportional to  $\nabla \epsilon$  should contribute to dissipation.

### 4. Dissipation Potentials

We propose a model of dissipation based on the dissipation potentials from classical mechanics [GPS14]. The corresponding dissipative forces are obtained by adding velocity-based gradients of these potentials to the Euler-Lagrange equations. We start this section with a formulation of dissipation potentials from strain energy densities, which after integration on discrete elements yield discrete dissipation potentials. Through this formulation, the forces on Eulerian and Lagrangian coordinates are derived in a sound way. We conclude the section with a derivation of force Jacobians for implicit integration.

#### 4.1. Strain Energy Dissipation

For a generic potential dissipation rate  $\dot{V}$ , dissipative forces can be added to the Euler-Lagrange equations as the negative gradient of the potential dissipation rate w.r.t. velocities, i.e.,  $\mathbf{f}_d = -\nabla_{\mathbf{q}} \dot{V}$ . Then, we obtain the dissipative version of the Euler-Lagrange equations:

$$\dot{\mathbf{M}} \ddot{\mathbf{q}} = \nabla T - \nabla V - \nabla_{\mathbf{q}} \dot{V} - \dot{\mathbf{M}} \dot{\mathbf{q}}. \quad (5)$$

Let us consider a generic strain energy density  $\frac{1}{2} k_e \epsilon^2$ . By integrating this energy density on a discrete element of size  $\Omega$ , we obtain the discrete elastic energy  $V$  in (2). By substituting strain with strain rate in the energy density, and applying the appropriate damping coefficient  $k_d$ , we can define a strain energy density dissipation rate  $\frac{1}{2} k_d \dot{\epsilon}^2$ . By integrating this energy dissipation rate on a discrete element, we obtain the discrete dissipation potential:

$$\dot{V} = \frac{1}{2} \Omega k_d \dot{\epsilon}^2. \quad (6)$$

For the subsequent derivations, it is convenient to identify the velocity-based gradient of the strain rate  $\dot{\epsilon}$ . Applying the chain rule, we get  $\dot{\epsilon} = \nabla \epsilon^T \dot{\mathbf{q}}$ . Then, by differentiating this expression, we obtain

$$\nabla_{\mathbf{q}} \dot{\epsilon} = \nabla \epsilon. \quad (7)$$

## 4.2. Eulerian-Lagrangian Dissipative Forces and Jacobians

From the generic definition of the discrete dissipation potential (6) and the velocity-based gradient of strain-rate (7), we obtain the dissipative forces:

$$\mathbf{f}_d = -\nabla_{\dot{\mathbf{q}}}\dot{V} = -\Omega k_d \dot{\epsilon} \nabla \epsilon. \quad (8)$$

For implicit integration, we derive the Jacobians of dissipative forces w.r.t. generalized positions and velocities:

$$\frac{\partial \mathbf{f}_d}{\partial \mathbf{q}} = -\Omega k_d (\dot{\epsilon} \mathbf{I} + \nabla \epsilon \dot{\mathbf{q}}^T) \mathbf{H} \epsilon - k_d \dot{\epsilon} \nabla \epsilon \nabla \Omega^T. \quad (9)$$

$$\frac{\partial \mathbf{f}_d}{\partial \dot{\mathbf{q}}} = -\Omega k_d \nabla \epsilon \nabla \epsilon^T. \quad (10)$$

The expression  $\mathbf{H} \epsilon$  denotes the Hessian of the strain w.r.t. the generalized coordinates.

For efficiency, we wish to solve the linear system resulting from backward-Euler implicit integration using a fast CG solver. However, the CG solver requires a symmetric matrix for guaranteed convergence, and the Jacobian of dissipative forces w.r.t. positions (9) contains non-symmetric terms. As suggested by Baraff and Witkin [BW98] we omit the non-symmetric terms altogether. In practice, as demonstrated by our results, we have not suffered any convergence problems. The approximate but symmetric Jacobian is:

$$\frac{\partial \mathbf{f}_d}{\partial \mathbf{q}} \approx -\Omega k_d \dot{\epsilon} \mathbf{H} \epsilon. \quad (11)$$

## 5. Yarn-Level Dissipation

In this section, we describe the application to the yarn-level cloth model [CLMMO14] of the dissipation potentials presented in the previous section. In particular, we develop the formulation for stretch, bending, and shear dissipation. In all cases, we build on previously defined discrete elastic potentials according to (2), and we explicitly identify strain  $\epsilon$  and element size  $\Omega$  in those formulations to derive corresponding dissipation potentials based on strain rate  $\dot{\epsilon}$ , according to (6). The derivation of dissipative forces and Jacobians would follow immediately as described in Section 4.2. For angular strains, such as bending or shear, we have recognized that dissipative forces suffer from indeterminacy at small angles. We propose a vector form of bending and shear strain for small angles, which is free of indeterminacy, and whose dissipation potential smoothly blends into the regular dissipation potential based on scalar forms of strain.

In the rest of this section, we refer to the notation defined in Fig. 2 for yarn segments. Fig. 2-left denotes two consecutive yarn segments that bend with angle  $\theta$  at node  $\mathbf{q}_0$ , and Fig. 2-right denotes two crossing yarn segments that shear with angle  $\phi$  at node  $\mathbf{q}_0$ . We define as  $\Delta \mathbf{x}_i = \mathbf{x}_i - \mathbf{x}_0$  the Lagrangian position difference between node  $\mathbf{q}_0$  and an adjacent node, and we define as  $\Delta u_i = u_i - u_0$  the arc-length difference between node  $\mathbf{q}_0$  and an adjacent node.

### 5.1. Stretch

A stretch potential models the opposition of a yarn segment to change its length. For the yarn segment between  $\mathbf{q}_0$  and  $\mathbf{q}_1$ , the

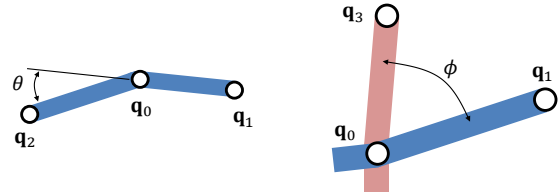


Figure 2: Notation employed in the derivation of strain and strain-rate metrics for yarn-level cloth. Left: two consecutive yarn segments that bend with angle  $\theta$  at node  $\mathbf{q}_0$ . Right: two crossing yarn segments that shear with angle  $\phi$  at node  $\mathbf{q}_0$ .

stretch potential is defined by the following strain and segment size:

$$\epsilon = |\mathbf{w}| - 1, \quad \text{with } \mathbf{w} = \frac{\Delta \mathbf{x}_1}{\Delta u_1}, \quad (12)$$

$$\Omega = \Delta u_1. \quad (13)$$

Taking the time-derivative of the strain, we obtain the expression of the strain rate as a function of generalized velocities:

$$\dot{\epsilon} = \frac{\mathbf{w}^T}{|\mathbf{w}|} \frac{\Delta \dot{\mathbf{x}}_1 - \mathbf{w} \Delta \dot{u}_1}{\Delta u_1}. \quad (14)$$

### 5.2. Bending

Bending forces model the opposition of two consecutive yarn segments to bending deformation. We define a bending strain metric based on the angle between such pair of consecutive segments, as shown in Fig. 2-left:

$$\epsilon = \frac{\theta}{\Delta u_1 - \Delta u_2}, \quad \text{with } \tan \theta = \frac{|\Delta \mathbf{x}_2 \times \Delta \mathbf{x}_1|}{-\Delta \mathbf{x}_2^T \Delta \mathbf{x}_1}, \quad (15)$$

$$\Omega = \Delta u_1 - \Delta u_2. \quad (16)$$

From this expression, the strain rate expressed as a function of the generalized velocities is:

$$\dot{\epsilon} = \frac{\dot{\theta} - \epsilon (\Delta \dot{u}_1 - \Delta \dot{u}_2)}{\Delta u_1 - \Delta u_2}, \quad (17)$$

with

$$\dot{\theta} = -\frac{\cos^2 \theta}{\Delta \mathbf{x}_2^T \Delta \mathbf{x}_1} \left( (\Delta \mathbf{x}_2^T \Delta \dot{\mathbf{x}}_1 + \Delta \mathbf{x}_1^T \Delta \dot{\mathbf{x}}_2) \tan \theta + \frac{(\Delta \mathbf{x}_2 \times \Delta \mathbf{x}_1)^T}{|\Delta \mathbf{x}_2 \times \Delta \mathbf{x}_1|} (\Delta \mathbf{x}_2 \times \Delta \dot{\mathbf{x}}_1 - \Delta \mathbf{x}_1 \times \Delta \dot{\mathbf{x}}_2) \right). \quad (18)$$

Unfortunately, under vanishing angles, the strain gradient is undefined. This is not a problem for elastic forces (3), because the undefined gradient is multiplied by the vanishing strain. However, for the dissipative force in (8), a non-zero strain rate at a zero-strain configuration produces a force with undefined direction.

We handle vanishing angles differently, thanks to the small-angle approximation of the tangent, i.e.,  $\lim_{\theta \rightarrow 0} \frac{\tan \theta}{\theta} = 1$ . In particular, we define the following vector strain metric for small bending angles:

$$\epsilon = \frac{\mathbf{v}}{\Delta u_1 - \Delta u_2}, \quad \text{with } \mathbf{v} = \frac{\Delta \mathbf{x}_2 \times \Delta \mathbf{x}_1}{-\Delta \mathbf{x}_2^T \Delta \mathbf{x}_1}. \quad (19)$$

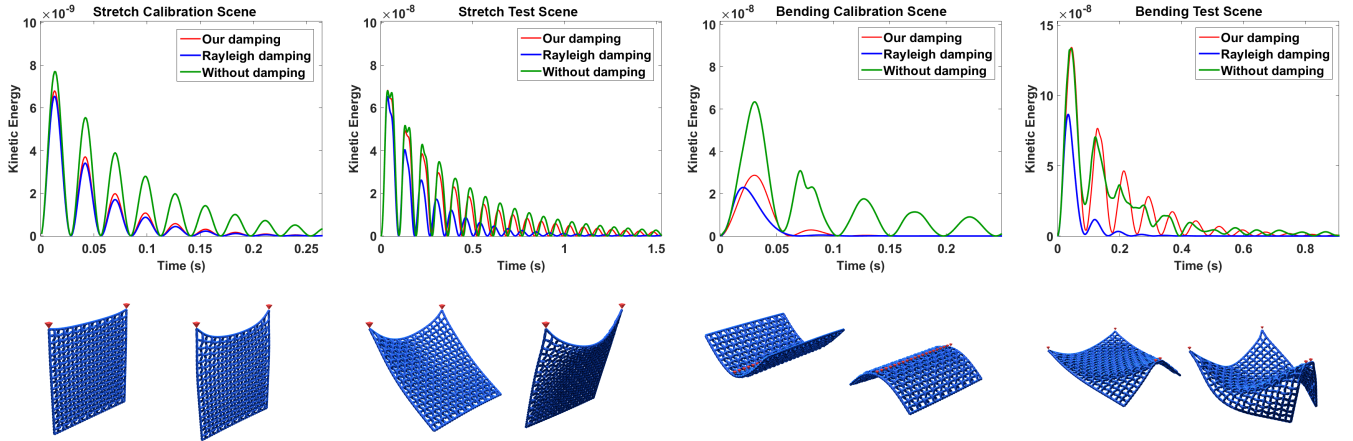


Figure 3: The plots demonstrate the ability of our model to control the damping behavior of each deformation mode independently, unlike Rayleigh damping. For each deformation mode (i.e., stretch or bending), we tune the damping parameters of our model and Rayleigh damping to produce the same damped behavior on a calibration scene, which is dominated by the mode under study. Then, using the same parameters, we run a test scene, which is dominated by other modes. From left to right, plots of kinetic energy for the stretch calibration scene, stretch test scene, bending calibration scene, and bending test scene, respectively. The two snapshots below each plot depict the configuration of the corresponding scene. Gravity is turned off in the bending calibration scene. The behavior of our model is most similar to Rayleigh damping on the calibration scenes, as expected, but it is most similar to the no-damping configuration on the tests scenes, demonstrating the ability to control the behavior of each deformation mode independently.

The elastic potential  $V$  in (2) is defined based on the squared norm of the strain vector. Then, from (19) and (15), we have  $V \propto \tan^2 \theta$ , which for small angles yields  $V \propto \theta^2$ . We conclude that our regular and small-angle bending potentials are equivalent under small angles. Note that the small-angle bending strain metric is not well suited for large angles, as it tends to infinity.

In contrast to the regular bending strain (15), the small-angle bending strain (19) has a well-defined gradient for vanishing angles. Therefore, it enables robust computation of dissipative forces. Taking the time-derivative of the strain vector in (19), we reach the small-angle bending strain-rate:

$$\dot{\varepsilon} = \frac{\dot{\mathbf{v}} - \varepsilon (\Delta\mathbf{u}_1 - \Delta\mathbf{u}_2)}{\Delta\mathbf{u}_1 - \Delta\mathbf{u}_2}, \quad (20)$$

with

$$\dot{\mathbf{v}} = -\frac{1}{\Delta\mathbf{x}_2^T \Delta\mathbf{x}_1} ((\Delta\mathbf{x}_2^T \Delta\dot{\mathbf{x}}_1 + \Delta\mathbf{x}_1^T \Delta\dot{\mathbf{x}}_2) \mathbf{v} + \Delta\mathbf{x}_2 \times \Delta\dot{\mathbf{x}}_1 - \Delta\mathbf{x}_1 \times \Delta\dot{\mathbf{x}}_2). \quad (21)$$

In our implementation, we use the small-angle bending strain metric for angles smaller than 5 degrees.

### 5.3. Shear

At yarn crossings, shear of crossing yarns, as shown in Fig. 2-right, produces a deformation of the yarns due to contact. This effect was modeled by Cirio et al. [CLMMO14] using a shear potential based on the shear angle  $\phi$ . This shear potential uses the following metrics of strain and element size:

$$\varepsilon = \phi - \frac{\pi}{2}, \quad (22)$$

$$\Omega = L, \quad (23)$$

where  $L$  is the rest-state distance between adjacent yarns.

For vanishing shear angles, the strain gradient is undefined, as it suffers the same problem discussed above for the bending strain gradient. We fix this problem by defining a vector strain metric for small shear angles, analogous to the solution proposed for bending strain.

## 6. Results

We have tested our damping model on the woven cloth simulation approach of Cirio et al. [CLMMO14]. We integrate the equations of motion numerically using an implicit backward Euler scheme with a single Newton step, and we solve the resulting linear equation system using the implementation of the CG method provided by Eigen [GJ\*10]. Our simulations are executed on the CPU for testing purposes. Moreover, in order to validate our derivations, we have compared implementations using both analytical and finite-difference derivatives, reaching equivalent results.

We continue this section by discussing the experimental validation of the success of our damping model. First, we have validated that our model enables independent tuning of the damping behavior for the different deformation modes. Second, we have quantified this independence by evaluating the damping ratio on animation sequences that excite different deformation modes. Finally, we have analyzed the success of the model to produce realistic damping behavior on large-scale examples. The simulation parameters of all our experiments are listed in Table 1. A time step of 1 ms and a mass density of 130 kg/m<sup>3</sup> were used in all cases.



Figure 4: Square piece of cloth dropped on top of a sphere. In the video we compare the damping behavior with different damping models.



Figure 5: Mannequin wearing a tank top. In the video we compare the damping behavior under different parameters of our model.

### 6.1. Control of Damping Behavior

We have designed small-scale experiments where we evaluate the ability of our model to tune the damping behavior of each deformation mode independently. In addition, we have compared the performance of Rayleigh damping on the same experiments. Specifically, we have tested stretch and bending dissipation. We omit the shear deformation mode from these tests, due to the difficulty of designing an experiment dominated by shear deformation.

For each deformation mode (i.e., stretch or bending), we design a calibration scene and a test scene. The calibration scene is dominated by motion along the deformation mode under study, while the test scene is dominated by motion on other deformation modes. The snapshots in Fig. 3 depict the calibration and test scenes for stretch and bending deformation modes.

For the mode under study, we tune the damping coefficients of our model ( $k_d$ ) and Rayleigh damping ( $\beta$ ) to reach a similar damped behavior on the calibration scene. We do not apply damping on the other deformation modes. Then, we run the test scene using the same parameters. A well-behaved damping model would produce minimal damping on the test scene.

The plots in Fig. 3 compare the kinetic energy with our model, Rayleigh damping, and no damping. From left to right, the plots refer to the stretch calibration scene, the stretch test scene, the bending calibration scene, and the bending test scene. In the calibration scenes, the behavior of our model and Rayleigh damping is similar, as expected. In the test scenes, on the other hand, our model succeeds to exhibit a behavior similar to the no-damping configuration, while Rayleigh damping produces undesired damped behavior.

### 6.2. Damping Ratio

We have also quantified the damping behavior on the scenes described in the previous section. Specifically, we fit a characteristic second-order oscillatory function to the kinetic energy plot, and thus compute the *damping ratio*, a dimensionless metric that describes how oscillations in a system decay after a perturbation. The

characteristic function of an oscillatory second-order system is:

$$f(t) = 2e^{-\omega_n \zeta t} \cos\left(\omega_n t \sqrt{1 - \zeta^2}\right), \quad (24)$$

where  $\omega_n$  is the natural frequency and  $\zeta$  is the damping ratio.

The plots in Fig. 6 evaluate the effect on the damping ratio in the stretch calibration and test scenes as we vary the stretch damping coefficient  $k_d$ . For our model, the damping ratio of the calibration scene grows with higher  $k_d$ , as expected, but the damping ratio of the test scene remains close to constant. For Rayleigh damping, on the other hand, the damping ratio in both scenes grows with higher  $k_d$ . Again, the analysis of the damping ratio demonstrates that our model clearly outperforms Rayleigh damping in its ability to control the damping behavior of each deformation mode independently.

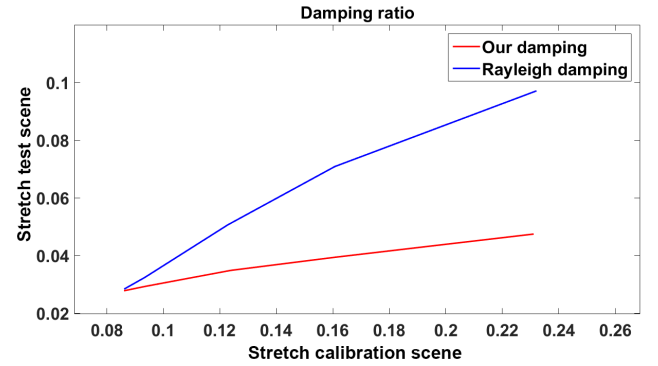


Figure 6: The plots depict the damping ratio on the stretch calibration and test scenes, as we vary the stretch damping coefficient  $k_d$ . For our model, the damping ratio of the calibration scene grows with higher  $k_d$ , as expected, but the damping ratio of the test scene remains close to constant. For Rayleigh damping, on the other hand, the damping ratio in both scenes grows with higher  $k_d$ .

Scenes	Nodes	Seg. length	Yarn radius	$k_e$		$k_d$		Rayleigh $\beta$
				Stretch	Bending	Stretch	Bending	
Stretch test (Fig. 3)	400	1mm	0.25mm	$5 \times 10^2$	$10^{-5}$	$3 \times 10^{-7}$	0	$4 \times 10^{-3}$
Bending test (Fig. 3)	380	1mm	0.25mm	$5 \times 10^2$	$10^{-5}$	0	$10^{-13}$	$3 \times 10^{-2}$
Sphere (Fig. 4)	40,000	0.57mm	0.16mm	$10^4$	$10^{-3}$	$10^{-5}$	$10^{-12}$	$5 \times 10^{-2}$
Tank top underdamped (Fig. 5)	22,121	4mm	1.15mm	$10^4$	$10^{-3}$	$10^{-6}$	$10^{-14}$	-
Tank top cr. damped (Fig. 5)	22,121	4mm	1.15mm	$10^4$	$10^{-3}$	$10^{-3}$	$10^{-10}$	-
Tank top overdamped (Fig. 5)	22,121	4mm	1.15mm	$10^4$	$10^{-3}$	$10^{-1}$	$10^{-6}$	-
Tank top kick (Fig. 1)	22,121	4mm	1.15mm	$10^6$	$10^{-3}$	$5 \times 10^{-2}$	$10^{-9}$	-

Table 1: Simulation parameters of all the scenes shown in the paper.

### 6.3. Large-Scale Examples

We have also evaluated the impact of the proposed damping model on large-scale simulation examples. Please see the dynamics effects on the accompanying video.

In Fig. 4 we show a piece of cloth that is dropped on a sphere. The size of the cloth is  $11.5 \times 11.5$  cm, and it consists of 200 × 200 nodes. In this scene, we compare the behavior of our model, Rayleigh damping, and no damping.

Fig. 5 shows a male mannequin wearing a tank top with various degrees of damping, all simulated using our model. It is possible to obtain very diverse damping behaviors, ranging from clearly underdamped to overly damped. Fig. 1 shows the same mannequin wearing the same, but stiffer, tank top. The motion of the garment remains nicely damped even under fast motion of the mannequin, yet the fabric retains rich folds and wrinkles.

The simulation results have been rendered with the Unity game engine. We use Catmull-Rom interpolation to smooth the curve defined by the simulation nodes, and we then generate a tube-shaped mesh per yarn for visualization.

## 7. Conclusion

In this paper, we have presented a formulation of dissipative forces for yarn-level cloth simulation. Our method is general and can be applied to all the elastic potentials that characterize cloth mechanics, and we have shown its successful application to stretch, bending and shear. In the future, we would like to extend the model to other elastic potentials, in particular those present in knitted cloth [CLMO17]. It would also be interesting to explore the application of dissipation potentials to other simulation models, beyond yarn-level cloth. Our formulation of dissipation potentials offers two major advantages in contrast to the dissipative forces of Baraff and Witkin [BW98]: it supports arbitrary types of generalized coordinates, and it enables resolution-independent parameterization of the dissipative behavior, as it is derived from energy density principles.

We have demonstrated that our model enables independent control of the damping behavior of the various deformation modes. In particular, we have demonstrated that the model outperforms the classic Rayleigh damping model. We would like to evaluate the behavior on models of even higher resolution. To this end, the model

must be implemented on the GPU to increase its computational efficiency.

To conclude, we would like to explore the estimation of damping coefficients from real-world measurements.

### Acknowledgements

The authors wish to thank the anonymous reviewers for their feedback, as well as the members of the MSLab at URJC for their support. In particular, Gabriel Cirio for immense help with the yarn-level cloth simulation framework, Juanjo Casafranca for early research on dissipation potentials, Carlos Castillo and Jorge López for rendering support, and Héctor Barreiro for demo production. This work was funded in part by the European Research Council (ERC Proof-of-Concept grant 713742 FabricMetrics) and the Spanish Ministry of Economy (grant TIN2015-70799-R and a corresponding FPI fellowship).

### References

- [BD13] BENDER J., DEUL C.: Adaptive cloth simulation using corotational finite elements. *Computers & Graphics* 37 (2013), 820–829. [2](#)
- [BJ05] BARBIĆ J., JAMES D. L.: Real-time subspace integration for st. venant-kirchhoff deformable models. *ACM Trans. Graph.* 24, 3 (July 2005), 982–990. [1](#)
- [BW98] BARAFF D., WITKIN A.: Large steps in cloth simulation. In *Proceedings of the 25th annual conference on Computer graphics and interactive techniques* (1998), ACM, pp. 43–54. [1, 2, 3, 4, 7](#)
- [CK05] CHOI K.-J., KO H.-S.: Stable but responsive cloth. In *ACM SIGGRAPH 2005 Courses* (2005), ACM, p. 1. [2](#)
- [CLMMO14] CIRIO G., LOPEZ-MORENO J., MIRAUT D., OTADUY M. A.: Yarn-level simulation of woven cloth. *ACM Trans. Graph.* 33, 6 (2014), 207:1–207:11. [1, 2, 3, 4, 5](#)
- [CLMO15] CIRIO G., LOPEZ-MORENO J., OTADUY M. A.: Efficient simulation of knitted cloth using persistent contacts. In *Proceedings of the 14th ACM SIGGRAPH/Eurographics Symposium on Computer Animation* (2015), pp. 55–61. [1, 2](#)
- [CLMO17] CIRIO G., LOPEZ-MORENO J., OTADUY M. A.: Yarn-level cloth simulation with sliding persistent contacts. *IEEE Transactions on Visualization and Computer Graphics* 23, 2 (2017), 1152–1162. [1, 2, 3, 7](#)
- [CYTT92] CARIGNAN M., YANG Y., THALMANN N. M., THALMANN D.: Dressing animated synthetic actors with complex deformable clothes. In *ACM Siggraph Computer Graphics* (1992), vol. 26, ACM, pp. 99–104. [2](#)

- [GBO04] GOKTEKIN T. G., BARGTEIL A. W., O'BRIEN J. F.: A method for animating viscoelastic fluids. *ACM Trans. Graph.* 23, 3 (2004), 463–468. [1](#)
- [GHDS03] GRINSPUN E., HIRANI A. N., DESBRUN M., SCHRÖDER P.: Discrete shells. In *Proceedings of the 2003 ACM SIGGRAPH/Eurographics symposium on Computer animation* (2003), Eurographics Association, pp. 62–67. [2](#)
- [GJ\*10] GUENNEBAUD G., JACOB B., ET AL.: Eigen v3. <http://eigen.tuxfamily.org>, 2010. [5](#)
- [GPS14] GOLDSTEIN H., POOLE C. P., SAFKO J. L.: *Classical Mechanics: Pearson New International Edition*. Pearson Higher Ed, 2014. [1](#), [2](#), [3](#)
- [GSS\*15] GAST T. F., SCHROEDER C., STOMAKHIN A., JIANG C., TERAN J. M.: Optimization integrator for large time steps. *IEEE Transactions on Visualization and Computer Graphics* 21, 10 (2015), 1103–1115. [1](#)
- [KJM08] KALDOR J. M., JAMES D. L., MARSCHNER S.: Simulating knitted cloth at the yarn level. *ACM Trans. Graph.* 27, 3 (2008), 65:1–65:9. [1](#)
- [KJM10] KALDOR J. M., JAMES D. L., MARSCHNER S.: Efficient yarn-based cloth with adaptive contact linearization. *ACM Trans. Graph.* 29, 4 (2010), 105:1–105:10. [1](#)
- [KYT\*06] KHAREVYCH L., YANG W., TONG Y., KANSO E., MARDEN J. E., SCHRÖDER P., DESBRUN M.: Geometric, variational integrators for computer animation. In *Proceedings of the 2006 ACM SIGGRAPH/Eurographics Symposium on Computer Animation* (2006), pp. 43–51. [1](#)
- [OAW06] OH S., AHN J., WOHN K.: Low damped cloth simulation. *The Visual Computer* 22, 2 (2006), 70–79. [2](#)
- [OSG02] O'BRIEN J. F., SHEN C., GATCHALIAN C. M.: Synthesizing sounds from rigid-body simulations. In *Proceedings of the 2002 ACM SIGGRAPH/Eurographics Symposium on Computer Animation* (2002), pp. 175–181. [1](#)
- [PICT15] PEER A., IHMSEN M., CORNELIS J., TESCHNER M.: An implicit viscosity formulation for sph fluids. *ACM Trans. Graph.* 34, 4 (2015), 114:1–114:10. [1](#)
- [Ray96] RAYLEIGH J. W. S. B.: *The theory of sound*, vol. 2. Macmillan, 1896. [2](#)
- [SSF13] SU J., SHETH R., FEDKIW R.: Energy conservation for the simulation of deformable bodies. *IEEE Transactions on Visualization and Computer Graphics* 19, 2 (2013), 189–200. [1](#)
- [TPBF87] TERZOPoulos D., PLATT J., BARR A., FLEISCHER K.: Elastically deformable models. In *ACM Siggraph Computer Graphics* (1987), vol. 21, ACM, pp. 205–214. [2](#)
- [VMT00] VOLINO P., MAGNENAT-THALMANN N.: Implementing fast cloth simulation with collision response. In *Computer Graphics International* (2000), vol. 2000, pp. 257–266. [2](#)
- [VMT01] VOLINO P., MAGNENAT-THALMANN N.: Comparing efficiency of integration methods for cloth simulation. In *Computer graphics international 2001. Proceedings* (2001), IEEE, pp. 265–272. [2](#)
- [YKC00] YU W., KANG T., CHUNG K.: Drape simulation of woven fabrics by using explicit dynamic analysis. *Journal of the Textile Institute* 91, 2 (2000), 285–301. [2](#)